PINN and KAN Temperature Prediction of Carbon Fiber/Epoxy Composite Materials Irradiated by Nuclear Explosion Simulated Light Source

Xiaoxiang Han [1,2,3], Jun li[1], Lin Yuan[1,2,3], Xin Zhang[1], Weijie Zhu[1], Yang Liu[1,2,3], Haiyang Zhang[1,2,3], Boyu Wang [1,2,3*]

1School of science, Xi'an Polytechnic University, Xi'an Shaanxi, 710048, China,

2 Engineering Research Center of Flexible Radiation Protection Technology, Universities of Shaanxi Province, Xi'an Polytechnic University, Xi'an 710048, Shaanxi, China，

3 Xi'an Key Laboratory of Nuclear Protection Textile Equipment Technology, Xi'an Polytechnic University, Xi'an 710048, Shaanxi, China.

** Corresponding author: wangby2008@foxmail.com*

Abstract

Carbon fiber/epoxy composite materials are extensively utilized in military, aerospace, and medical sectors due to their numerous advantages, including light weight, high toughness, and corrosion resistance. The investigation of their thermal effects is crucial for enhancing their resilience to extreme environments. Based on experimental data obtained from nuclear explosion simulated light irradiation experiments, a fast solver based on the physical information neural network (PINN) was developed and implemented. The Kolmogorov Arnold network (KAN) was employed to analyze and predict the correlation between multiple experimental parameters and the material's surface temperature. A heat conduction model encompassing the entire process from irradiation to cooling was proposed. The PINN method was utilized to analyze the material temperature changes, resulting in a fast solution model for the spatiotemporal evolution of material temperature. An in-depth analysis was conducted on the influence of various experimental parameters on the maximum surface temperature and its occurrence time. By constructing a dataset of each parameter and the target temperature, an efficient KAN prediction model was achieved, capable of establishing explicit functional relationships between input parameters and T_{max}, t_{max}. The KAN prediction model exhibits high interpretability. An ensemble learning strategy was adopted to integrate the six deep learning models for prediction, thereby enhancing the robustness of the prediction results. This study presents a PINN and KAN temperature prediction model of carbon fiber/epoxy composite materials irradiated by nuclear explosion simulated light source, offering thermal protection solutions for equipment based on carbon fiber/epoxy composite materials in nuclear explosion scenarios.

Keywords: Nuclear Explosion, Optical radiation; Carbon fiber/epoxy composite; Physical information neural network; Kolmogorov Arnold network;

Introduction

Composite materials boast high specific strength, high specific modulus, and erosion resistance, making them widely applicable in critical fields such as military, medical, aviation, and navigation. Consequently, they must withstand high temperatures and drastic temperature changes induced by weapon explosions and strong light radiation during operation. When subjected to strong light radiation, the high heat generated by the radiation severely impacts the integrity of composite material structures (ablation, delamination, rapid degradation of mechanical properties). Traditional methods like the Finite Difference Method (FDM) and Finite Element Method (FEM) face challenges in refining differential mesh, optimizing iteration step size, managing diverse error sources, and ensuring computational efficiency when solving the complex physical phenomenon of the heat radiation equation. Therefore, the study of temperature evolution in composite materials under strong light radiation, rapid calculation of material surface temperature, and rapid prediction of surface characteristics remains a challenging yet vital task.

Over the past few decades, researchers have extensively explored the physical mechanisms of materials under strong light radiation, proposing various partial differential equations (PDEs) for heat conduction to describe the temperature evolution process of laser action on different material regions over time [1]-[8]. For instance, Qin Y et al. established an axisymmetric mathematical model for long pulse Nd: YAG laser heating of aluminum alloy plate, utilizing the finite element method to calculate the temperature and thermal stress inside the plate [1]. Song Guowen et al. examined the temperature evolution of heat conduction under low radiation [2], while Chen et al. investigated the effect of laser irradiation on carbon fiber reinforced resin composites under tangential airflow load [3]. Li W et al. studied nonlinear heat transfer during the decomposition and surface ablation processes of charcoal burning materials [4], and Askarizadeh et al. conducted precise analysis of two-dimensional Fourier and non-Fourier biological heat transfer equations under skin tissue exposure to instantaneous heating conditions [5]. Su et al. utilized the finite difference method to simulate the transmission and storage of energy in a firefighter protective suit model under low-intensity thermal radiation [6], and Tian Mingwei et al. developed a heat

transfer model for a microsystem comprising thermal protective clothing, air gaps, and multiple layers of human skin, numerically solving the temperature evolution using the finite element method [7]. Li X et al. explored the volume ablation phenomenon of carbon fiber composite materials by continuous high-power density laser, proposing a one-dimensional transient model to analyze temperature evolution and material pyrolysis [8].

Despite significant advancements in the study of materials under radiation effects using traditional methods, which have provided a clearer understanding of the effects of different radiation parameters on material temperature evolution and thermal damage, these studies are all based on grid-based numerical solutions, which are time-consuming and cannot be quickly reused. With the rapid advancement of artificial intelligence technology, a series of cutting-edge prediction and optimization algorithms have emerged, deeply penetrating key fields such as biomedicine, intelligent technology, image recognition, automation control, and even the solution of complex physical phenomena like partial differential equations. Innovative methods such as Physics Informed Neural Networks (PINNs), Kolmogorov Arnold Networks (KANs), and Deep Operator Networks (DeepONet) are leading a new trend in scientific research [13]-[22]. Cai S et al. investigated the application of PINN in various prototype heat transfer problems, considering different thermal boundary conditions on the heating surface, and obtained the temperature and velocity fields of the internal region under different boundary conditions [13]. Based on PINN, Lu Zhibin et al. studied the two-dimensional steady-state thermal conductivity equation of the internal heat source and the two-dimensional steady-state convective heat transfer equation between flat plates, achieving a fast surrogate model to predict the temperature field output [14]. He et al. proposed a data-driven framework based on PINNs, which achieved heat transfer analysis and parameter inversion for heat conduction problems [15]. Wang et al. introduced a Multi Domain Physical Information Neural Network (mPINN) to solve non-uniform heat conduction and conjugate natural convection problems with discontinuous temperature gradients at interfaces [16]. Bowman et al. used PINN to study the interaction between laser and biological tissue, analyzing the physical neural network with source term heat equation under different boundary conditions [17]. Billah Md Muhtasim et al. explored a PINN to estimate unknown thermophysical parameters for inverse heat transfer in planar walls of conductive materials [18]-[20]. Li X et al. investigated a

method for identifying non-uniform thermal diffusivity using temperature data collected from transient heat conduction problems using a hybrid PINN [21]. Lu et al. provided a Python library (DeepXDE) that contributes to the faster development of research in the field of machine learning [22]. Recently, KAN prediction model is introduced to analyze the relationship between different parameters and material surface temperature characteristics [23]. The KAN model is mainly inspired by the Kolmogorov Arnold representation theorem, and replaces fixed activation functions with learnable activation functions on the edges ("weights"), which more effectively approximates nonlinear functions while maintaining a smaller network size. KAN has interpretability advantages, visualizes the learned spline functions, and allows researchers to gain a deeper understanding of the potential mathematical or physical laws captured by the model. KAN is particularly attractive for scientific discoveries of new physical laws and can easily interact with human users for predictive analysis [24-26]. In previous studies, most of them used PINN to study single-layer radiative heat transfer models, only considering the radiation stage without considering the cooling stage. Therefore, research in this area is urgently needed.

Here， we uses PINN to establish a fast prediction model for the temperature evolution of carbon fiber/epoxy composite materials irradiated by nuclear explosion simulated light sources, and uses KAN for interpretable analysis of different parameters to predict the temperature characteristics of the material. A radiation and cooling model for carbon fiber/epoxy composite materials irradiated by nuclear explosion simulated light sources was established. Based on the surface temperature data, a PINN fast prediction model was constructed to obtain the implicit function mapping relationship between the input spatiotemporal domain and the output temperature. The relationship between different parameters and the highest temperature on the back surface, as well as the corresponding time of this temperature, was analyzed. The KAN neural network was used for training and prediction, and the learnable activation function curve and visualization relationship on the edge were obtained. This comprehensive approach not only leverages the strengths of PINN for rapid and accurate temperature prediction but also integrates the interpretability of KAN to provide deeper insights into the underlying physical processes. By combining these advanced computational techniques with traditional methods, this study significantly advances the understanding and application of carbon fiber/epoxy composite

materials in extreme environments, particularly in scenarios involving nuclear explosion light radiation. The findings contribute to the development of more robust thermal protection solutions, enhancing the durability and reliability of composite materials in critical applications.

Methods

Radiation and cooling model of carbon fiber/epoxy composite material

The radiation and cooling model of carbon fiber/epoxy composite materials describes the behavior of these materials under the influence of a simulated nuclear explosion light source. Initially, the epoxy resin undergoes thermal decomposition due to the rapid increase in temperature. As the temperature reaches the maximum thermal decomposition temperature of the carbon fiber materials, surface carbonization occurs, leading to further surface ablation with continued irradiation. When the irradiation ceases, the carbon fiber/epoxy composite material cools naturally. During the early cooling phase, the front surface temperature remains higher than the back surface, continuing to transfer heat to the back surface until the back surface reaches its maximum temperature.

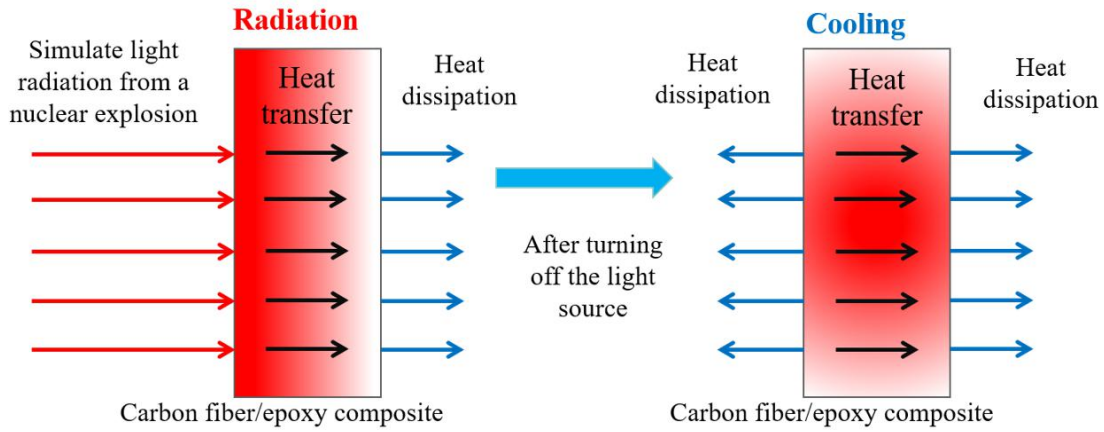

Fig. 1 Light radiation and cooling model of carbon fiber/epoxy composite

In order to describe the dynamics process, a radiation and cooling model was established here. The specific model is shown in Fig. 1, and can be given as followed：

$$\begin{aligned} \rho c\frac{\partial T}{\partial t} &= \frac{\partial}{\partial x}\left(k\frac{\partial T}{\partial x}\right)+\gamma q_{red}e^{-\gamma x} \qquad 0<t<t_{\exp} \\ \rho c\frac{\partial T}{\partial t} &= \frac{\partial}{\partial x}\left(k\frac{\partial T}{\partial x}\right) \qquad t_{\exp}<t \\ \gamma &= -ln(\tau)/L \end{aligned} \tag{1}$$

Where, T represents the sample temperature; k, ρ and c represent the thermal conductivity, density, and specific heat capacity of carbon fiber/epoxy composite materials, respectively; γ is the front surface extinction coefficient; q_{red} represents the energy density of simulated light source; t_{exp} is the duration of light radiation acts on the sample surface; τ is the outer layer transmittance; L is the sample thickness. The boundary and initial conditions of the radiation and cooling model are defined based on thermal convection and radiation principles in heat transfer, expressed as:

$$\begin{aligned}
&-k\left.\frac{\partial T}{\partial x}\right|_{x=0} = \alpha q_{red} - h_f(T_q - T_0) - \varepsilon\delta(T_q^4 - T_0^4) \qquad 0 < t < t_{\text{exp}} \\
&-k\left.\frac{\partial T}{\partial x}\right|_{x=0} = -h_f(T_q - T_0) - \varepsilon\delta(T_q^4 - T_0^4) \qquad t_{\text{exp}} < t \\
&-k\left.\frac{\partial T}{\partial x}\right|_{x=L} = h_f(T_L - T_0) + \varepsilon\delta(T_L^4 - T_0^4) \qquad 0 < t \\
&T\big|_{t=0} = T_0 \qquad T\big|_{t=t_{\text{exp}}} = T_{\text{exp}}(x)
\end{aligned} \tag{2}$$

Where, α is the proportionality coefficient of heat conduction energy absorption; H_{f} is the air convection coefficient; T_{q} and T_{L} are the front and back surface temperatures, respectively; ε is the surface emissivity; T_0 is the ambient temperature; T_{exp} is the temperature at different positions during t_{exp}; δ is the Stefan Boltzmann constant. The air convection coefficient is primarily influenced by wind speed, expressed as：

$$h_f = 0.08Ma^{0.8} = 0.08\left(\frac{v}{v_s}\right)^{0.8} \tag{3}$$

Where, Ma is the Mach number; v is the wind speed; V_{s} is the speed of sound. Employing the finite difference method, the radiation and cooling model equations, along with their boundary and initial conditions, are numerically solved. The model is discretized as：

$$\begin{aligned}
&T_j^{n+1} = T_j^n + \left[\frac{k}{\rho c\Delta x^2}(T_{j+1}^n + T_{j-1}^n - 2T_j^n) + \frac{\gamma q_{red}}{\rho c}e^{-\gamma x_j}\right]\Delta t \qquad 0 < n \le \frac{t_{\text{exp}}}{\Delta t} \\
&T_j^{n+1} = T_j^n + \left[\frac{k}{\rho c\Delta x^2}(T_{j+1}^n + T_{j-1}^n - 2T_j^n)\right]\Delta t \qquad \frac{t_{\text{exp}}}{\Delta t} < n
\end{aligned} \tag{4}$$

Then, the boundary and initial conditions are discretized as：

$$
\begin{aligned}
T_1^{n+1} &= T_2^{n+1} - \left(\frac{h_f (T_1^n - T_0) + \varepsilon\delta((T_1^n)^4 - T_0^4) - \beta q_{red}}{k} \right) \Delta x \qquad 0 < n \le \frac{t_{\exp}}{\Delta t} \\
T_1^{n+1} &= T_2^{n+1} - \left(\frac{h_f (T_1^n - T_0) + \varepsilon\delta((T_1^n)^4 - T_0^4)}{k} \right) \Delta x \qquad \frac{t_{\exp}}{\Delta t} < n \\
T_{end}^{n+1} &= T_{end-1}^{n+1} - \left(\frac{h_f (T_{end}^n - T_0) + \varepsilon\delta((T_{end}^n)^4 - T_0^4)}{k} \right) \Delta x \qquad 0 < n \\
T_j^1 &= T_0 \qquad\qquad T_j^{\frac{t_{\exp}}{\Delta t}} = T_{\exp}(x)
\end{aligned}
\tag{5}
$$

Where, Δx and Δt represent the step size for thickness and time, respectively. j is the thickness coordinate of the discrete point, and n is the time axis coordinate. Divided into radiation and cooling processes, the discrete equations are calculated to obtain the temperature evolution of the sample.

PINN based Radiation and Cooling Model

With advancements in artificial intelligence, PINNs have been introduced in computational physics to directly solve partial differential equations. PINNs train neural networks to solve supervised learning tasks while adhering to physical laws described by general nonlinear partial differential equations, avoiding traditional grid differencing through a meshless method. This allows for the storage of trained physical network parameters, facilitating quick approximate parameter problem solving. Based on the finite difference method for the proposed radiation model, PINN is utilized for specific coefficient network training, constructing a fast PINN network solver under specific coefficients. PINN comprises perceptron, deep neural network, automatic differentiation, and physical information components. The basic PINN concept involves using neural networks to train input spatiotemporal domains and output characteristics, obtaining partial derivatives of output characteristics relative to independent variables to construct the physical model's loss function. Optimization algorithms then adjust network parameters to minimize mean square error and other evaluation indicators, satisfying the established physical model.

For the proposed radiation and cooling model, PINN analysis is conducted based on finite difference method and experimental data, establishing a series of PINN fast solvers to minimize the loss function. The solver includes two neural networks for radiation and cooling, two automatic differential structures, and two optimization loss function optimizers, with the specific

solving structure illustrated in Figure 2. The inputs to the networks are location and time, with temperature as the output. Using physical constraints, initial condition constraints, and boundary condition constraints of the radiation model, the PINN loss function is defined as：

$$loss_{\mathrm{R}}=\frac{1}{N_{\mathrm{R}}}\sum_{i=1}^{N_{\mathrm{R}}}\left|\frac{\partial T(x,t)}{\partial t}-\frac{k}{\rho c}\frac{\partial^2 T(x,t)}{\partial x^2}-\gamma q_{red}e^{-\gamma x}\right|^2 \qquad loss_{\mathrm{b}}=\frac{1}{N_{\mathrm{b}}}\sum_{j=1}^{N_{\mathrm{b}}}\left|T^j-T(x_{\mathrm{b}}^j,t_{\mathrm{b}}^j)\right|^2$$

$$loss_{\mathrm{C}}=\frac{1}{N_{\mathrm{C}}}\sum_{i=1}^{N_{\mathrm{C}}}\left|\frac{\partial T(x,t)}{\partial t}-\frac{k}{\rho c}\frac{\partial^2 T(x,t)}{\partial x^2}\right|^2 \qquad loss_{\mathrm{d}}=\frac{1}{N_{\mathrm{d}}}\sum_{j=1}^{N_{\mathrm{d}}}\left|T^j-T(x_{\mathrm{d}}^j,t_{\mathrm{d}}^j)\right|^2$$

$$Loss=loss_{\mathrm{R}}+loss_{\mathrm{b}}+loss_{\mathrm{C}}+loss_{\mathrm{d}} \tag{6}$$

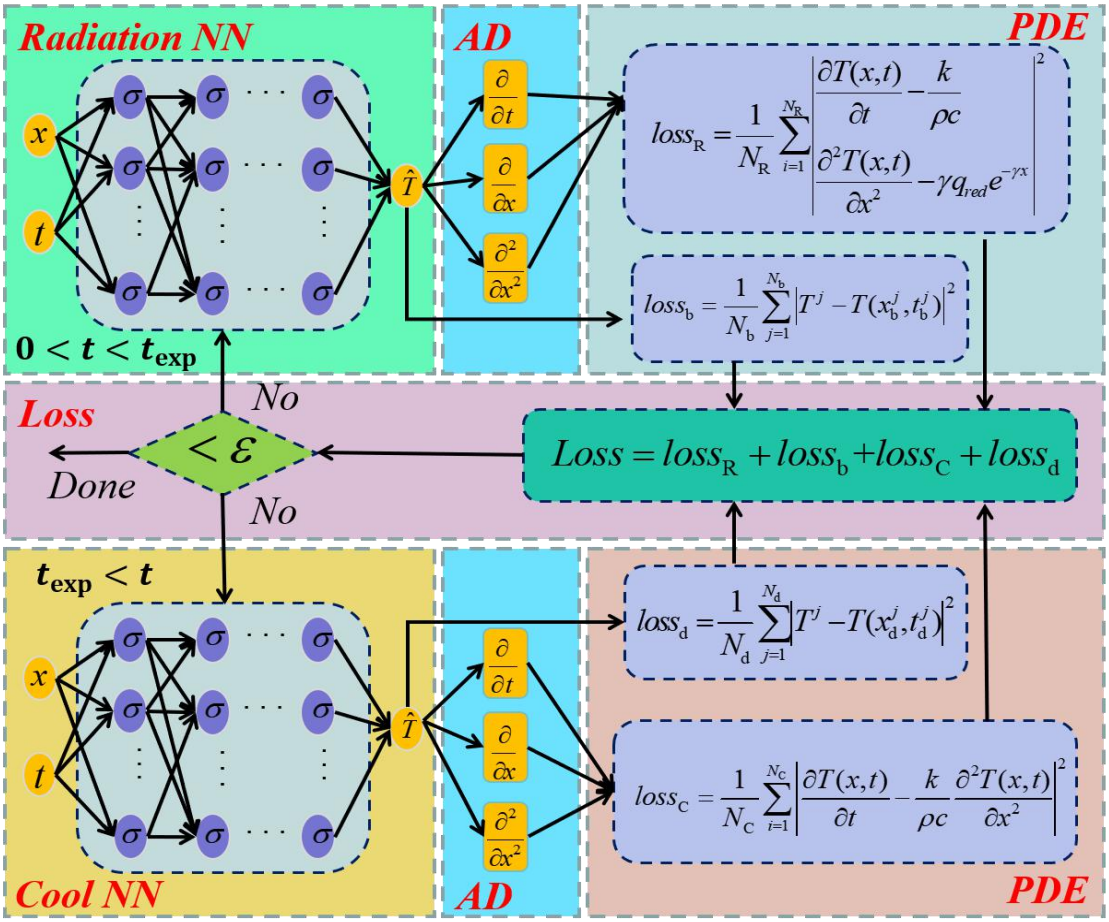

Fig. 2 Physical information neural network (PINN) diagram of radiation and cooling model

Where, T (x, t) is the temperature at position x and time t, N_{R} and N_{C} are the number of internal points for radiation and cooling, N_{b} and N_{d} are the sum of initial and boundary points for radiation and cooling. $loss_{\mathrm{R}}$ and $loss_{\mathrm{C}}$ are the physical constraint residual terms for radiation and cooling, which are used to satisfy the network information of the radiation model. $loss_{\mathrm{b}}$ and $loss_{\mathrm{d}}$ are residual terms constraining the initial and boundary conditions of the two stages, ensuring the

neural network meets these conditions. *Loss* is the overall loss function of the radiation model. By minimizing *Loss* with an optimizer, an approximate solution to the radiation model Eq. (1) is obtained, efficiently predicting any position in the spatiotemporal domain through multiple matrix multiplications in the trained feedforward neural network, achieving a nonlinear mapping between the spatiotemporal domain and the temperature field. This process eliminates dependence on computational grids, significantly enhancing numerical analysis efficiency, with numerical solutions expressed using implicit function relationships for more efficient analysis and simulation of carbon fiber/epoxy composite material temperature changes.

KAN Temperature Feature Prediction Model

During the radiation and cooling experiments, the back surface temperature of samples and its corresponding time have always been of great concern. In order to clearly determine the back surface temperature and its corresponding time under different parameter conditions, we conducted a large number of numerical simulations on the modified radiation simulation model and created a dataset. Introducing KAN for interpretable prediction of temperature characteristics corresponding to different parameters, where KAN uses spline parameterized univariate functions instead of traditional linear weights, enabling it to dynamically learn activation patterns and significantly improve interpretability. The specific structure is shown in Figure 3, where the activation function is placed on the edge rather than the node. The Kolmogorov Arnold representation theorem states that any multivariate continuous function can be represented as a finite combination function of continuous single variables and binary addition operations, allowing complex functions to be decomposed into simpler and more interpretable parts. Its theorem is expressed as：

$$f(x) = f(x_1, x_2, ..., x_n) = \sum_{q=1}^{2n+1} \Phi_q \left(\sum_{p=1}^{n} \phi_{q,p}(x_p) \right) \tag{7}$$

$\phi_{q,p}$ is a univariate function that maps each input variable x_{p}. ϕ_{q} is a continuous function, where ϕ_{q} is the function matrix corresponding to the q_{th} KAN layer. The specific matrix expression is as follows: the function $f(x)$ is represented as the composite of the inner and outer function matrices applied to the input vector x, expressed as:

$$f(x) = \Phi_{\mathrm{out}} \circ \Phi_{\mathrm{in}} \circ x \tag{8}$$

Among them, ϕ_{m} is a matrix of univariate function, represented as：

$$\Phi_{\text{in}}=\begin{pmatrix}\phi_{1,1}(\cdot) & \cdots & \phi_{1,n}(\cdot)\\ \vdots & & \vdots\\ \phi_{2n+1,1}(\cdot) & \cdots & \phi_{2n+,n}(\cdot)\end{pmatrix} \tag{9}$$

ϕ_{out} is the row vector of a univariate function：

$$\Phi_{\text{out}}=(\Phi_1(\cdot)\cdots\Phi_{2n+1}(\cdot)) \tag{10}$$

These matrices illustrate a Kolmogorov Arnold layer that forms the basis of KAN by stacking these layers. Therefore, the construction of KAN is as follows：

$$\text{KAN}(x)=(\Phi_{L-1}\circ\Phi_{L-2}\circ\cdots\circ\Phi_1\circ\Phi_0)x \tag{11}$$

KAN is based on this theory, replacing fixed activation functions with learnable activation functions at the edges (weights). KAN replaces fixed activation functions with learnable spline-based activation functions, enabling it to approximate complex nonlinear functions more effectively than traditional models such as BP and RF. This enables KAN to model complex interactions in high-dimensional data through simpler combinations of univariate functions. In addition, the visualization of KAN is simple, with each layer resembling a fully connected layer, where each edge contains a one-dimensional function, simplifying the understanding of complex networks through the direct representation of functional layers. This model allows for deeper and more interpretable connections between input features and outputs, demonstrating the potential for enhancing model transparency in machine learning applications. KAN uses extracted symbolic formulas to enable us to understand the potential relationship between input features and results. Its excellent predictive accuracy and interpretability make it a promising alternative to traditional machine learning models in predicting the surface temperature and corresponding time during the radiation and cooling experiments.

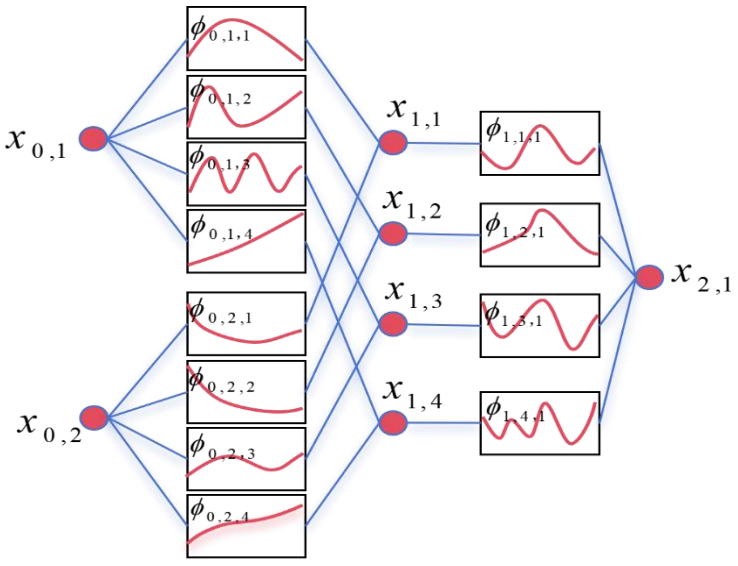

Fig. 3 Structure diagram of Kolmogorov Arnold network (KAN)

Results and discussion

Experimental measurement

Figure 3 shows the KAN structure, which is analyzed through experimental measurement simulation. By using a temperature sensor to measure the front and back surface temperatures of sample and repeating the above testing steps and measure the front and back surface temperatures of samples with thicknesses of 2, 4, 5.7, and 6 mm, the temperature changes of samples are shown in Table 1. able 1 provides the temperature measurement data of carbon fiber/epoxy composite in light experiments caused by light radiation from a nuclear explosion simulation light source.

Table 1 Temperature of carbon fiber/epoxy composite during radiation from nuclear explosion simulation light source

Measurement conditions	T(K)	Measurement conditions	T(K)
Initial temperature	293.04	Temperature at L=5.7mm and t=9s	309.14
Front surface temperature at t=9s	493	Temperature at L=6mm and t=9s	296.36
Temperature at L=2mm and t=9s	391.92	Maximum temperature at rear surface during cooling stage	300.87
Temperature at L=3mm and t=9s	361.61		

Based on the experimental data of carbon fiber/epoxy composite materials irradiated by nuclear explosion simulation light source, numerical solution was carried out using finite difference method. The parameters of simulation are as followed: ρ=1.562 g/cm^3, c=1.028 J/(g*K), k=0.745 W/(m*K), δ=5.67*10^{-8} W/(m^2*K^4), ε=0.4, γ=0.00001 mm^{-1}, q_{red}=10 W/cm^2, α=0.012, h_f=20.05 W/(m^2*K) and T_0=293.04 K. The simulation results are approximately the same as the experimental results. Therefore, the temperature dynamics of sample can be obtained in Fig. 4. Figures 4 (a) and (b) are 3D temperature evolution process and top view of the 3D temperature evolution process, respectively. It can be seen that the temperature gradually increases along the thickness direction when irradiated within 0-9 seconds. Within 9-18 seconds, the light source is turned off. Due to the effects of thermal convection and diffusion, the sample will undergo temperature diffusion along the thickness direction towards the rear surface, causing the rear surface temperature continue to rise to the highest value and then begin to decrease. Figure 4 (c) shows the temperature variation curves with different thicknesses. It can be seen that the temperature is rapidly rise during the irradiation stage. The front surface temperature reaches its maximum value after nine seconds of irradiation. The time for the maximum temperature to occur

at other thicknesses is greater than 9 seconds, and as the thickness increases, the time for the highest temperature to occur also increases. Figure 4 (d) shows the temperature variation curve with thickness at different time points. It can be seen that the temperature distribution with high value at the middle and low value at both sides will occur along the thickness direction during the cooling stage.

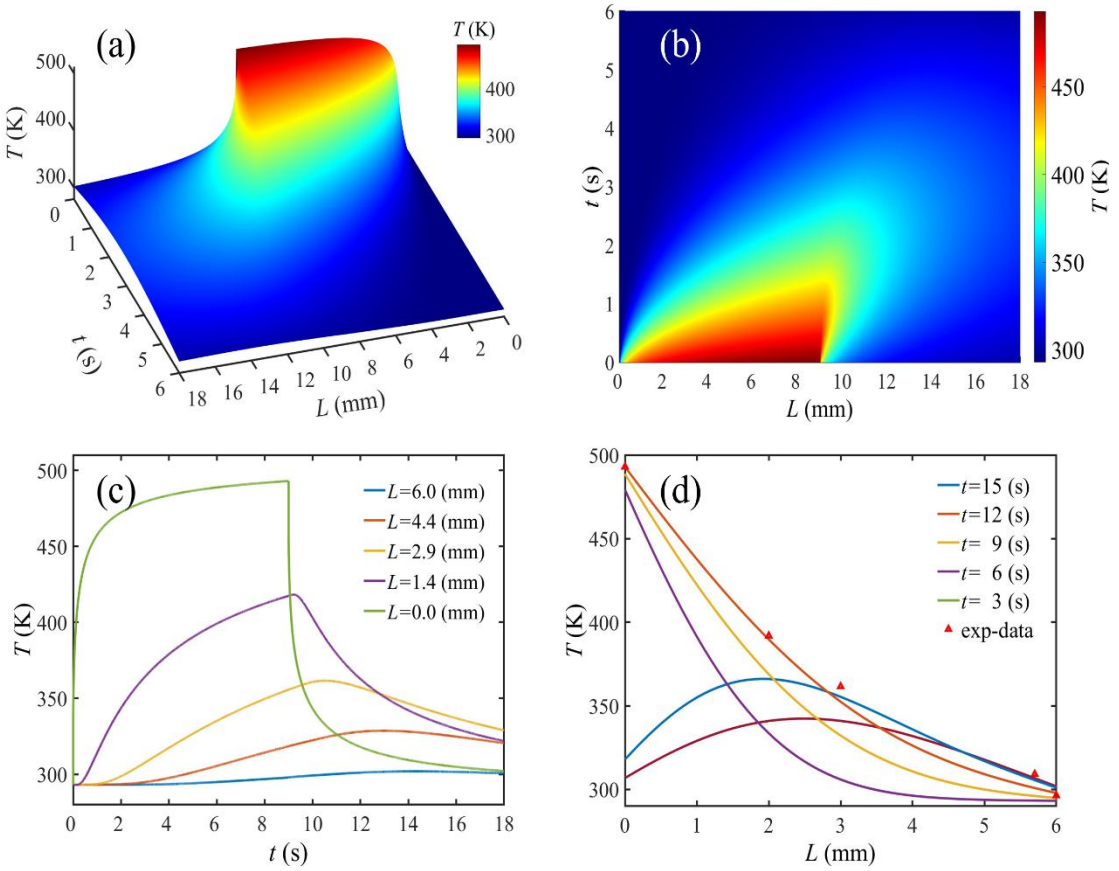

Fig. 4 Simulation results based on finite difference method (FDM). (a) 3D temperature evolution process; (b) Top view of the 3D temperature evolution process; (c) Temperature curves with respect to different thicknesses; (d) Temperature curve with respect to different time.

PINN Analysis of Radiation and Cooling Model

The implementation of PINN for the radiation and cooling model involves several key steps. First, a spatiotemporal coordinate system is established based on t and L. This system is crucial for accurately capturing the dynamics of the temperature evolution during the irradiation and cooling stages. Next, physical information for these stages is constructed, incorporating the relevant thermal properties and boundary conditions. The FDM is then employed to numerically solve the initial position, boundary position, and experimental data, which serve as the initial conditions and

boundary constraints corresponding to the physical information of PINN. Then, a PINN solver is constructed. The feedforward neural network for both the irradiation and cooling stages is configured with 2 neurons in the input layer, 20 neurons in the hidden layer, and 1 neuron in the output layer. The number of hidden layers, activation functions, weight initialization, and learning rate are all set to 4, tanh, Glorot normal, and 10^{-3}, respectively. The two network loss functions are optimized using Adam and L-BFGS to ensure they meet the physical information corresponding to the radiation and cooling models. Finally, the performance evaluation curve of the loss function for the radiation and cooling model is derived, and the trained PINN solver is completed. The proposed PINN solver enables the rapid acquisition of temperature evolution dynamics for both stages.

According to the aforementioned steps for PINN training, the results for the radiation and cooling model are illustrated in Figure 5. Figure 5(a) presents the spatiotemporal temperature evolution derived from PINN training using a mixture of finite difference method simulation data and experimental data. Figure 5(b) highlights the error between the training data and PINN prediction data, indicating that the primary error occurs at the boundary between the irradiation and cooling stages. The performance evaluation of PINN has been calculated. After 10,000 iterations of PINN in both stages, the training errors are 10^{-2} and 10^{-4}, respectively, signifying that the network associated with this PINN solver exhibits good generalization ability. The neural network employed for the radiation and cooling stages divides the spatiotemporal range into 1,540 small blocks for solving. The boundary sampling points of the spatiotemporal range are 160, and the sampling points for testing the accuracy of the solution results are 1,540. The number of optimization training steps is 8,000, and the time required to train the neural network is approximately 15 minutes. The speed of solving internal local points of the proposed heat conduction model based on the trained network is notably fast. For instance, solving 5,202 spatiotemporal position points through the trained model takes only 0.064 seconds, which is ten times faster than traditional methods. Additionally, this method does not involve grid partitioning and ignores errors generated during the iterative process, allowing it to solve the corresponding temperature in any spatiotemporal domain and quickly address a large number of repetitive and identical computational problems. This approach holds significant potential for the future

construction of a large model for rapid solving of heat transfer and temperature evolution prediction.

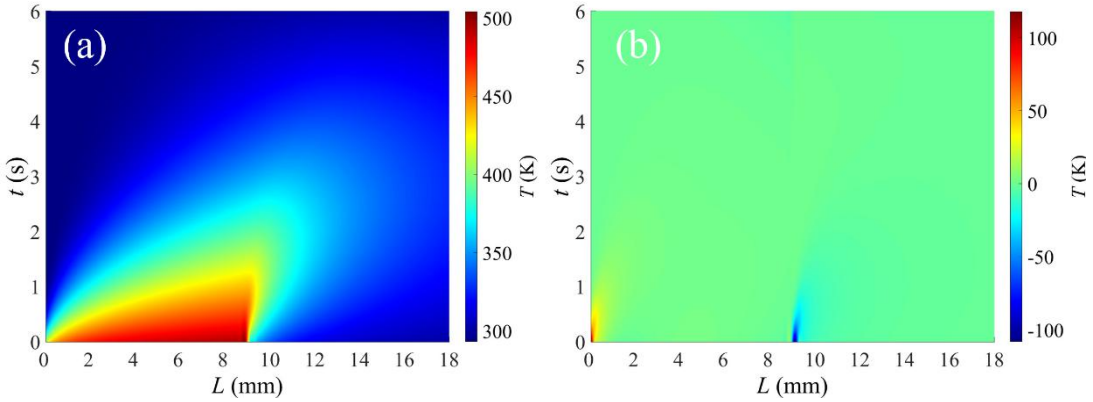

Fig. 5 Simulation results based on PINN. (a) Temperature evolution process; (b) Error between the PINN results and training sample.

Simulation calculation with different input parameters

In practical applications, the maximum surface temperature T_{max} and its corresponding time t_{max} have always been a focus of attention in the engineering field. In the experiment, the selection of various parameters is closely related to the highest temperature in the cooling stage. In order to better study the relationship between various parameters and the highest temperature in the cooling stage, as well as the time when this temperature occurs, and to provide better guidance for actual measurements, we used a modified experimental program to investigate the effects of changes in the initial temperature T_0 of carbon fiber/epoxy composite materials from 291.04 to 299.04 K, thickness L from 4.5 to 7.0 mm, energy density q_{red} of nuclear explosion simulation light sources from 8 to 10 W/cm^2, and the time t_{exp} of light source radiation on the surface of carbon fiber/epoxy composite materials from 7 to 12 s on the cooling stage. The influence of the maximum surface temperature T_{max} and its corresponding t_{max} was examined. Figure 6 shows the relationship between different input parameters and temperature characteristics. The insets in the Fig. 6 shows the variation of T_{max} and t_{max} with various parameters. Figure 6 (a) shows the temperature variation curves of the back surface corresponding to different energy densities. It can be seen that as q_{red} gradually increases, T_{max} gradually increases and t_{max} gradually decreases. Figure 6 (b) shows the temperature variation curves of the back surface corresponding to different initial temperature. As T_0 gradually increases, T_{max} also increases, while t_{max} remains unchanged. Figure 6 (c) depicts the temperature variation curves of the back surface corresponding to different thicknesses. As L increases, T_{max} gradually decreases and t_{max} gradually increases. Figure 6 (d)

illustrates the temperature variation curves of the back surface corresponding to different radiation times. As t_{exp} increases, both T_{max} and t_{max} also increase. Figure 6 clearly depicts the relationship between different input parameters and the maximum surface temperature and its corresponding time.

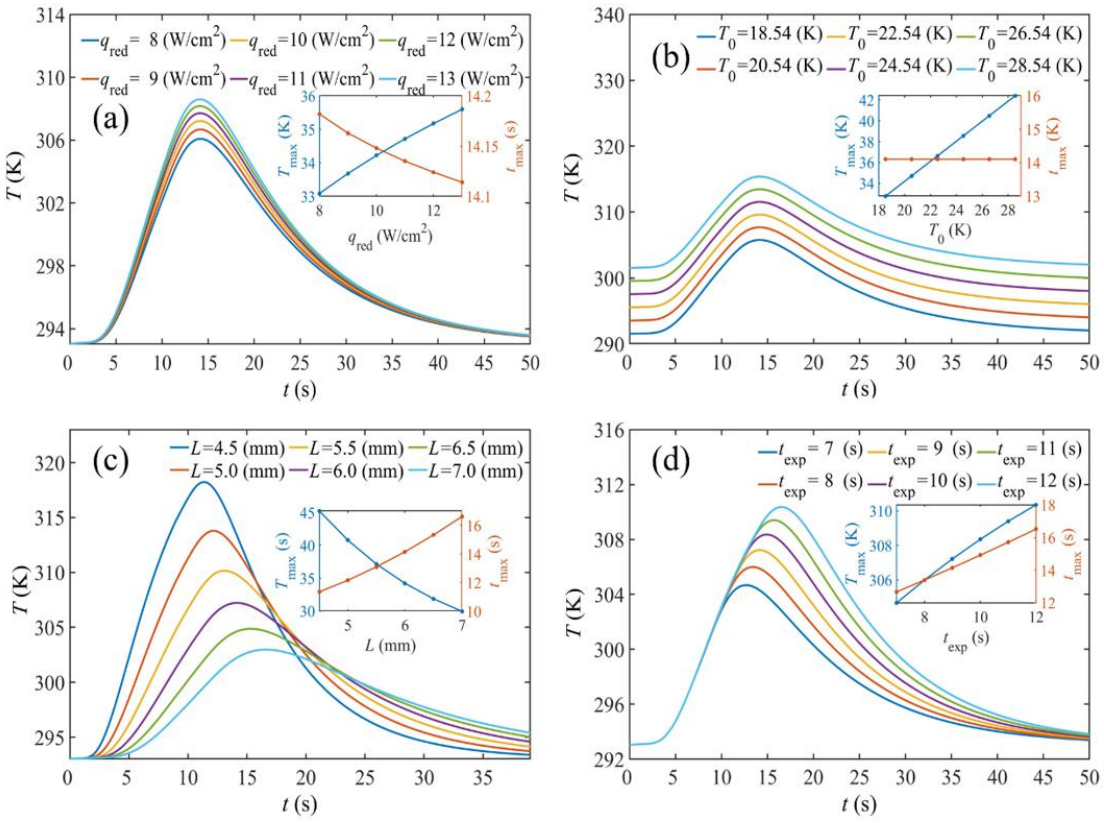

Fig. 6 Temperature variation with respect to different parameters, insets show the variation of T_{max} and t_{max} with respect to different parameters. (a) Temperature variation with respect to q_{red}, (b) Temperature variation with respect to T_0, (c) Temperature variation with respect to L, (d) Temperature variation with respect to t_{exp}.

Analysis of KAN Temperature Feature Prediction Model

To clearly predict the surface temperature corresponding to different parameters, an initial temperature T_0, thickness L, energy q_{red}, and the time t_{exp} were randomly assigned values within the simulated parameter variation range mentioned above. Other parameters followed Table 2, and the highest temperature T_{max} and the t_{max} were simulated. A sample dataset of 1,000 different input parameters and output results was generated and used to construct and train a KAN neural network for better analysis and prediction of the relationship between the effects of different parameters on the radiation surface temperature characteristics. Three aspects of analysis were specifically studied: visual prediction using the KAN network, comparison of multiple deep learning prediction algorithms with the KAN network prediction algorithms, and integrating

multiple prediction models into a multi-mechanism prediction model using the idea of ensemble learning to increase the stability of predictions.

To gain a deeper understanding of how the input parameters affect the maximum surface temperature, the KAN neural network was used for training and analysis. Firstly, we construct a fully connected KAN network structure, perform sparse regularization initial training on this structure to promote the sparsity of network weights, reduce model complexity, and prevent overfitting. Secondly, we use automatic pruning algorithm to identify and remove hidden neurons that contribute less to model prediction. This process not only reduces the size of the model, improves its computational efficiency and generalization ability, but also forms a more compact and efficient KAN model. Thirdly, all activation functions in the network were symbolized, allowing the network's behavior to be described in mathematical expressions, providing convenience for subsequent analysis and verification. Finally, we use the Sympy library to calculate the symbol formula of the output node and verify the correct answer. In order to comprehensively evaluate the predictive performance of the KAN model, Mean Absolute Error (MAE) and Root Mean Square Error (RMSE) were introduced as evaluation metrics. These two indicators can quantify the difference between the model's predicted values and the true values. Specifically, MAE measures the average size of prediction errors, while RMSE performs square weighting on errors and is more sensitive to outliers. The specific calculation formulas for the two indicators are as follows：

$$MAE = \frac{1}{N}\sum_{i=1}^{N}\left|\hat{A}_i - A_i\right| \qquad RMSE = \sqrt{\frac{1}{N}\sum_{i=1}^{N}\left(\hat{A}_i - A_i\right)^2} \tag{9}$$

The proposed KAN model is used to predict the maximum surface temperature after the cooling stage. The number of hidden layers, input neurons, output neurons, intermediate hidden neurons, grid spacing, and splines in the KAN configuration are set to 1, 4, 1, 2, 5, and 3, respectively. The LBFGS optimizer is used for training to simplify and explain the prediction of the maximum temperature based on the input parameters. The KAN training prediction step is shown in Figure 7, which clearly captures the complex nonlinear relationship between input features and output results. The symbol formula extracted in KAN provides further interpretability for predicting the maximum surface temperature after the cooling stage, allowing us to understand

the potential relationship and specific expression between the four parameters (initial temperature T_0, thickness L, energy q_{red}, the radiation time t_{exp}) and the maximum temperature T_{max}, and the KAN predictions are consistent with those found by simulation calculations with different input parameters. As the initial temperature T_0, the energy q_{red}, and the irradiation time t_{exp} increase, the maximum surface temperature T_{max} gradually increases. As the thickness L increases, the maximum surface temperature T_{max} gradually decreases.

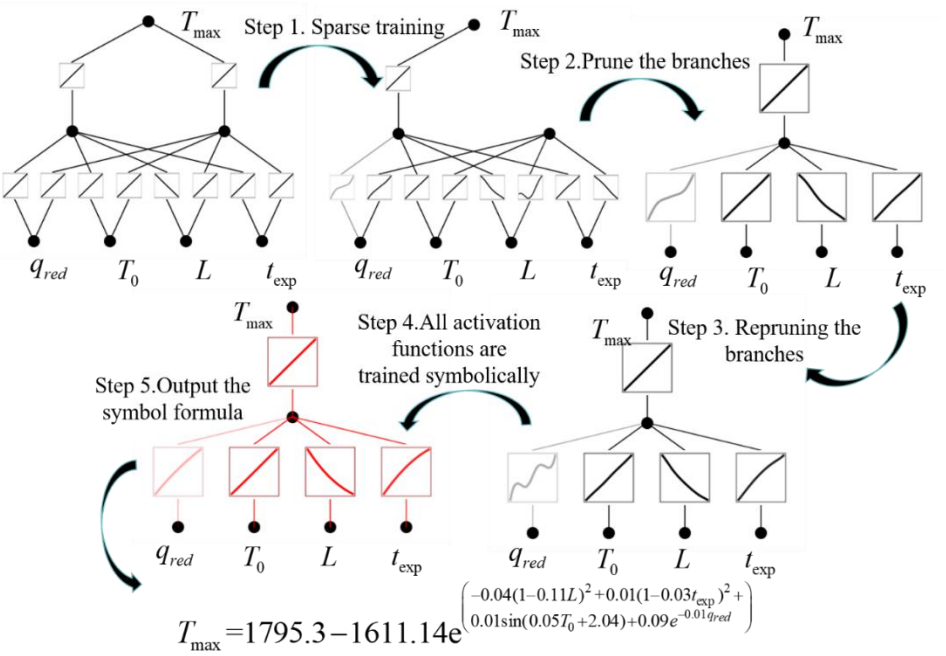

Fig. 7 KAN prediction model between the input parameters and T_{max}

The KAN model designed to predict the corresponding time of maximum surface temperature incorporates three hidden neurons within its intermediate layers. This architecture closely resembles that of the temperature prediction model, ensuring a consistent neural network structure. Following the same training procedures outlined in Figure 8, the Mean Absolute Error (MAE) and Root Mean Square Error (RMSM) for the predicted time of the highest surface temperature post-cooling stage are 0.1826 and 0.2306, respectively. Additionally, Figure 8 further illustrates the training steps of the second KAN model, revealing patterns in the input parameters that closely resemble those observed previously. By dissecting the one-dimensional functions associated with each edge, we gain insights into the functional relationships between various parameters and t_{max}. Notably, the initial temperature T_0 does not influence t_{max} , any initial temperature T_0 yields the same t_{max} .

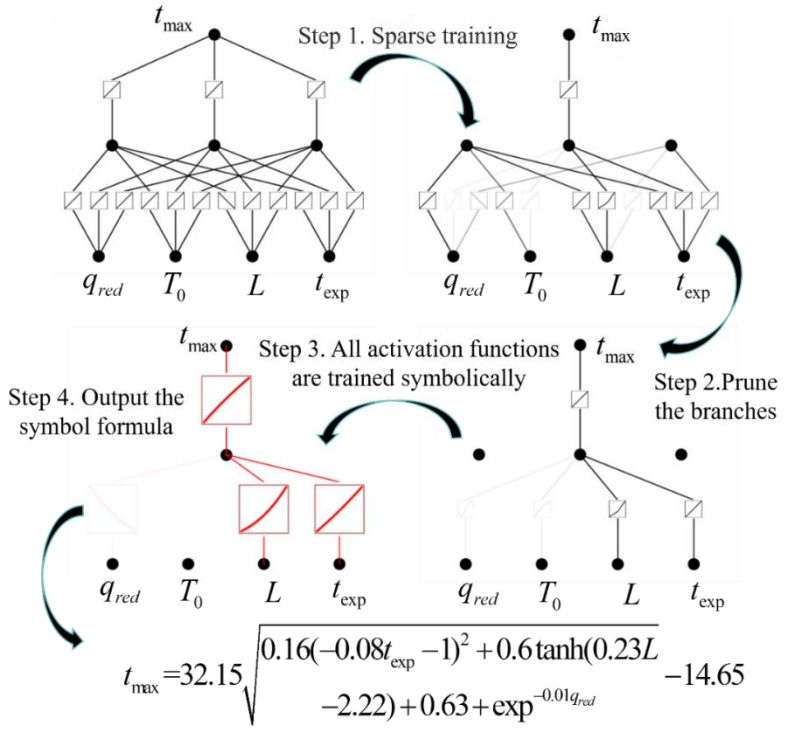

Fig. 8 KAN prediction model between the input parameters and t_{max}

The proposed KAN model stands out due to its innovative neural network structure, which enables it to approximate any continuous function with exceptionally high accuracy. This capability optimizes computing resources, solving highly complex nonlinear problems with minimal memory and computational power. Unlike traditional neural networks that often rely on deep stacking or extensive architectures to capture the nuances of complex functions, KAN employs a more compact and grounded framework. This innovation not only enhances the model's learning efficiency and prediction accuracy but also reduces its reliance on computational resources, making high-quality function approximation feasible even in resource-constrained environments. The suite of advantages offered by KAN represents a significant leap forward in traditional neural network design, offering fresh perspectives and methodologies for tackling complex physical phenomena, engineering challenges, and big data analytics. This suggests that artificial intelligence technology will exhibit broader application prospects and robust developmental potential across these domains.

To assess the performance of the proposed KAN model, we subjected it to a comparative analysis with traditional deep learning prediction models, utilizing a meticulously designed simulation dataset as our testing platform. In this predictive capacity competition, we enlisted six

representative models—SVM, ELM, RF, BP, RBFNN, and KAN—to comprehensively analyze and predict the temperature characteristics of the rear surface. To ensure a fair and accurate evaluation, we employed MAE and RMSE as our key performance indicators, executing 10 cycles of prediction algorithms for each model and averaging the results to achieve more stable outcomes. The specific prediction comparison outcomes are detailed in Table 2. It is evident from Table 3 that KAN, with its distinctive single-layer network structure, matches the accuracy of other models. Additionally, the table highlights the varying impacts of different deep learning models on prediction indicators, deepening our understanding of each model's characteristics and providing valuable insights for future performance prediction research in similarly complex environments.

Table 2 Comparison of prediction model results using different intelligent algorithms

Intelligent algorithms	T_{max}		t_{max}	
	MAE	RMSM	MAE	RMSM
KAN (1 layer)	0.4301	0.5383	0.1826	0.2306
BP (1 layer)	0.5055	0.6493	0.1855	0.2288
BP (2 layer)	0.2108	0.2522	0.1549	0.19498
SVM	0.1661	0.2068	0.0508	0.0644
ELM (5 node)	0.7872	0.9160	0.4204	0.5385
ELM (10 node)	0.7144	0.8254	0.2405	0.2901
RF (5 tree)	0.7662	0.9969	0.1876	0.2707
RF (10 tree)	0.6607	0.8431	0.1650	0.2207
RBFNN (1 rbf)	0.3884	0.7704	0.1191	0.2965
RBFNN (2 rbf)	0.1651	0.2187	0.0401	0.0497

In the study of intelligent algorithms prediction, we identified instability within the prediction process. To address this, we introduced ensemble learning and constructed a multi-mechanism prediction model that integrates the six distinct algorithms mentioned above. Each prediction model, owing to its unique prediction mechanisms, exhibits different biases and variances during training and varies in sensitivity to noise and abnormal data. Each model excels in capturing specific data features. The organic integration of these diverse models not only disperses errors potentially introduced by a single model but also leverages their complementarity to significantly enhance the overall model's robustness. This multi-model collaborative approach effectively reduces the dependence of prediction results on single model deviations, improving both accuracy and stability. When constructing this multi-mechanism prediction model, we adopted a refined weight allocation strategy based on key performance indicators such as MAE and RMSE. The performance of each model in the prediction task was evaluated, and appropriate weights were

assigned accordingly. This process ensures that the model integration can fully leverage the strengths of each model while minimizing their potential weaknesses, achieving a more comprehensive and accurate capture of the overall data trend. The specific weight allocation formula is as follows:

$$A = g_{\mathrm{RF}} A_{\mathrm{RF}} + g_{\mathrm{RBFNN}} A_{\mathrm{RBFNN}} + g_{\mathrm{FLW}} A_{\mathrm{FLW}} + g_{\mathrm{SVM}} A_{\mathrm{SVM}} + g_{\mathrm{BP}} A_{\mathrm{BP}} + g_{\mathrm{KAN}} A_{\mathrm{KAN}}$$
$$g_{\mathrm{RF}} = \frac{1/Q_{\mathrm{RF}}}{1/Q_{\mathrm{RF}} + 1/Q_{\mathrm{RBFNN}} + 1/Q_{\mathrm{FLW}} + 1/Q_{\mathrm{SVM}} + 1/Q_{\mathrm{BP}} + 1/Q_{\mathrm{KAN}}} \tag{10}$$

Where, g_{RF}, g_{RBFNN}, g_{FLW}, g_{SVM}, g_{BP}, g_{KAN} are the weights corresponding to the six algorithms, respectively. Q_{RF}, Q_{RBFNN}, Q_{FLW}, Q_{SVM}, Q_{BP}, Q_{KAN} are the error metrics corresponding to the six algorithms, respectively. A is the predicted values after ensemble learning. A_{RF}, A_{RBFNN}, A_{FLW}, A_{SVM}, A_{BP}, A_{KAN} are the predicted values corresponding to the six algorithms, respectively. By training and simulating the integrated algorithm using the above algorithm, the real and predicted values of the nuclear explosion radiation input parameters and the maximum surface temperature and corresponding time after the cooling stage are compared in Figure 9. Figures 9 (a) and (b) show the MAE and RMSM index values of the multi mechanism prediction model corresponding to the maximum surface temperature and its occurrence time, which are 0.1425, 0.1706, 0.0376, and 0.0461, respectively. It can be concluded that the algorithm has good stability, and the various indicators corresponding to the predicted values are better than those predicted by a single algorithm. This multi mechanism prediction model utilizes the power of ensemble learning to demonstrate strong generalization ability, achieving a dual improvement in prediction accuracy and stability.

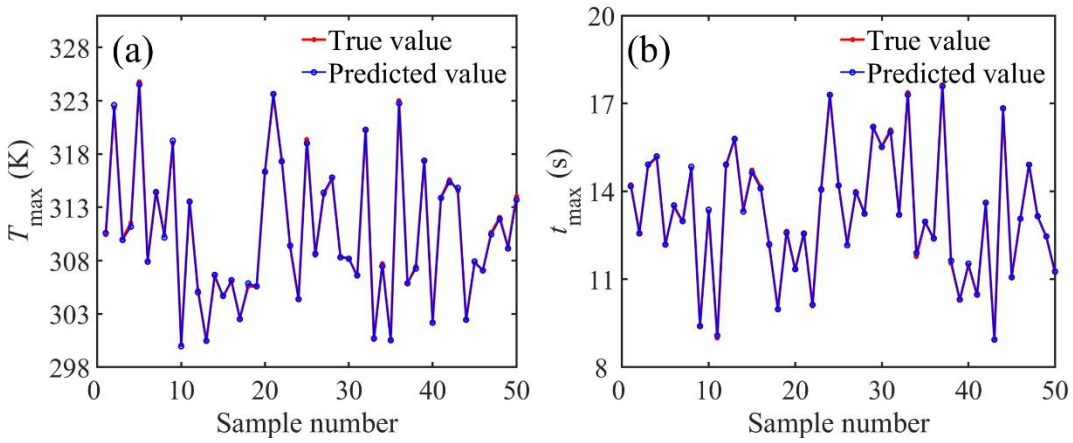

Fig. 9 Prediction value between multi-mechanism model and training sample, (a) Comparison between the training sample and predicted values of T_{max}, (b) Comparison between the training sample and predicted values of t_{max}.

Conclusion

We have successfully developed and implemented a rapid solver leveraging the PINN, and integrated the KAN to precisely forecast the correlation between the maximum surface temperature and its occurrence time, considering multiple parameters. A comprehensive mathematical model of heat conduction that encompasses both the radiation and cooling phases has been established. By amalgamating experimental data with model-solving data, PINN training effectively captures the implicit relationships between temperature and temporal-spatial variations, significantly enhancing computational efficiency in predicting temperature evolution. A detailed analysis was conducted to elucidate the influence mechanisms of various parameters on the maximum temperature and its timing on the rear surface. Subsequently, a meticulous parameter-temperature response database was constructed through numerical simulation. Capitalizing on KAN's superior accuracy, interpretability, and minimal hyperparameter requirements, an efficient prediction model was devised, yielding intuitive visual formulas that markedly enhance both readability and practicality of the model. To substantiate the superiority of the KAN model, we undertook a thorough comparative analysis against five prominent machine learning models—SVM, ELM, RF, BPNN, and RBFNN. Furthermore, to bolster the robustness of our prediction model, we adopted an ensemble learning approach, integrating six models for collaborative prediction. This strategy significantly augments the stability of prediction outcomes. This study not only employs PINN as an efficient tool for solving complex temperature evolution problems in carbon fiber/epoxy composite materials under simulated nuclear explosion radiation, but also trains a KAN model capable of accurately predicting peak temperatures and their corresponding times. This dual approach deepens our comprehension of its intrinsic operational mechanisms and predictive capabilities, which furnishes thermal protection solutions tailored for equipment constructed from carbon fiber/epoxy composites in nuclear explosion scenarios.

Acknowledgements

The authors acknowledge funding support from National Natural Science Foundation of China (Grant No.U2330109, 61805212), Natural Science Foundation of Shaanxi Province (2022JQ-660).

Author Declarations

Conflict of Interest

The authors have no conflicts to disclose.

Author Contributions

Xiaoxiang Han: Investigation (equal); Methodology (equal); Software (equal); Writing – original draft (equal); Writing – review & editing (equal). Jun Li: Methodology (equal); Writing – review & editing (equal). Lin Yuan: Writing – review & editing (equal). Xin Zhang: Writing – review & editing (equal). Weijie Zhu: Methodology (equal); Writing – review & editing

(equal). Yang Liu: Data curation (equal); Writing – review & editing (equal). Haiyang Zhang: Writing – review & editing (equal). Boyu Wang: Conceptualization (equal); Funding acquisition (equal); Resources (equal); Supervision (equal); Writing – review & editing (equal).

Data availability

The data that support the findings of this study are available from the corresponding author upon reasonable request.

References：

[1] Y. Qin, Y. Chen, X. Ni, et al., Axisymmetric numerical simulation of plastic damage in aluminum alloy induced by long pulsed laser. Optics and Lasers in Engineering 48(3), 361-367 (2010). https://doi.org/10.1016/j.optlaseng.2009.10.006

[2] G. Song, et al., Thermal protective performance of protective clothing used for low radiant heat protection," Textile Research J. 81(3), 311-323 (2011). https://doi.org/ 10.1177/0040517510380108

[3] M. Chen, H. Jiang, L. Jiao, et al., Study on the laser irradiation effects on carbon fiber rein forced resin composite subjected to tangential gas flow loading. 2nd International Symposium on Laser Interaction with Matter (LIMIS 2012). SPIE, 8796, 138-145 (2013). https://doi.org/ 10.1117/12.2011232

[4] W. Li, H. Huang, Y. Tian, et al., Nonlinear analysis on thermal behavior of charring materials with surface ablation. International Journal of Heat and Mass Transfer 84, 245-252 (2015). https://doi.org/ 10.1016/j.ijheatmasstransfer.2015.01.004

[5] H. Askarizadeh, H. Ahmadikia, Analytical study on the transient heating of a two-dimensional skin tissue using parabolic and hyperbolic bioheat transfer equations. Applied Mathematical Modelling 39(13), 3704-3720 (2015). https://doi.org/ 10.1016/j.apm.2014.12.003

[6] Y. Su, J. He, J. Li, Modeling the transmitted and stored energy in multilayer protective clothing under low-level radiant exposure. Applied Thermal Engineering 93, 1295-1303 (2016). https://doi.org/ 10.1016/j.applthermaleng.2015.10.089

[7] M. Tian, W. Song, L. Qu, S. Chen, et al., Thermal response of skin underneath a thermal protective garment during post-fire exposure. International Journal of Thermophysics 39, 1-17

(2018). https://doi.org/ 10.1007/s10765-018-2410-3

[8] X. Li, W. Hou, B. Han, et al., Thermal response during volumetric ablation of carbon fiber composites under a high intensity continuous laser irradiation. Surfaces and Interfaces 23, 101032 (2021). https://doi.org/ 10.1016/j.surfin.2021.101032

[9] R. Laubscher, Simulation of multi-species flow and heat transfer using physics-informed neural networks. Physics of Fluids 33(8), 087101 (2021). https://doi.org/10.1063/5.0058529

[10] G. E. Karniadakis, I. G. Kevrekidis, L. Lu, et al., Physics-informed machine learning. Nature Reviews Physics 3(6), 422-440 (2021). https://doi.org/ 10.1038/s42254-021-00314-5

[11] Y. Wang, J. Sun, J. Bai, et al., Kolmogorov Arnold Informed neural network: A physics-informed deep learning framework for solving PDEs based on Kolmogorov Arnold Networks. Computer Methods in Applied Mechanics and Engineering 433, 117518 (2025). https://doi.org/ 10.1016/j.cma.2024.117518

[12] L. Lu, P. Jin, G. Pang, et al., Learning nonlinear operators via DeepONet based on the universal approximation theorem of operators. Nat Mach Intell 3, 218-229 (2021). https://doi.org/ 10.1038/s42256-021-00302-5

[13] S. Cai, Z. Wang, S. Wang, et al., Physics-informed neural networks for heat transfer problems. Journal of Heat Transfer 143(6), 060801 (2021). https://doi.org/ 10.1115/1.4050542

[14] Z. Lu, J. Qu, H. Liu, et al., Surrogate modeling for physical fields of heat transfer processes based on physics-informed neural network. CIESC J. 72(3), 1496-1503 (2021). https://doi.org/ 10.11949/0438-1157.20201879 (in Chinese)

[15] Z. He, F. Ni, W. Wang, J. Zhang, A physics-informed deep learning method for solving direct and inverse heat conduction problems of materials. Materials Today Communications 28, 102719 (2021). https://doi.org/10.1016/j.mtcomm.2021.102719

[16] T. Wang, Z. Wang, Z. Huang, X. Guang, Multi-domain physics-informed neural network for solving heat conduction and conjugate natural convection with discontinuity of temperature gradient on interface. Sci. China Technol. Sci. 65, 2442-2461 (2022). https://doi.org/10.1007/s11431-022-2118-9

[17] B. Bowman, C. Oian, J. Kurz, et al., Physics-informed neural networks for the heat equation with source term under various boundary conditions. Algorithms 16(9), 428 (2023).

https://doi.org/ 10.3390/a16090428

[18] M. M. Billah, A. I. Khan, J. Liu, et al., Physics-informed deep neural network for inverse heat transfer problems in materials. Materials Today Communications 35, 106336 (2023). https://doi.org/ 10.1016/j.mtcomm.2023.106336

[19] S. M. Hosseini, T. Zarei and M. Pierantozzi, Modeling equilibrium and non-equilibrium thermophysical properties of liquid lubricants using semi-empirical approaches and neural network. Journal of Non-Equilibrium Thermodynamics 49(3), 289-307 (2024). https://doi.org/ 10.1515/jnet-2023-0062

[20] Zhu, T., Zheng, Q., and Lu, Y., Physics-Informed Fully Convolutional Networks for Forward Prediction of Temperature Field and Inverse Estimation of Thermal Diffusivity. ASME. J. Comput. Inf. Sci. Eng. 24(11), 111004 (2024). https://doi.org/ 10.1115/1.4064555

[21] X. Li, H. Chen, Z. Liu, Z. Yan and Z. Zhuang, Identifying varying thermal diffusivity of inhomogeneous materials based on a hybrid physics-informed neural network. International Journal of Applied Mechanics 14(07), 2250027 (2022). https://doi.org/ 10.1142/S1758825122500272

[22] L. Lu, X. Meng, Z. Mao, et al., DeepXDE: A deep learning library for solving differential equations. SIAM review 63(1), 208-228 (2021). https://doi.org/10.1137/19M1274067

[23] Z. Liu, Y. Wang, S. Vaidya, et al., Kan: Kolmogorov-arnold networks. arxiv preprint arxiv:2404.19756 (2024). https://doi.org/10.48550/arXiv.2404.19756

[24] Y. Peng, M. He, F. Hu, et al., Predictive Modeling of Flexible EHD Pumps using Kolmogorov-Arnold Networks. Biomimetic Intelligence and Robotics 4(4), 100184 (2024). https://doi.org/10.1016/j.birob.2024.100184

[25] H. Liu, J. Lei, Z. Ren, From Complexity to Clarity: Kolmogorov-Arnold Networks in Nuclear Binding Energy Prediction. arxiv preprint arxiv:2407.20737 (2024). https://doi.org/10.48550/arXiv.2407.20737

[26] M. Cheon, Kolmogorov-Arnold Network for Satellite Image Classification in Remote Sensing. arxiv preprint arxiv:2406.00600 (2024). https://doi.org/10.48550/arXiv.2406.00600